

Effects of contact shape on biological wet adhesion

Yewang Su · Baohua Ji · Yonggang Huang ·
Kehchih Hwang

Received: 18 December 2006 / Accepted: 10 April 2007 / Published online: 17 July 2007
© Springer Science+Business Media, LLC 2007

Abstract Wet adhesion is widely adopted in biological adhesion systems in nature. Wet adhesion is studied in this paper with the focus on the effect of different contact shapes (flat, concave, convex, and ring-like) on the adhesion force. The evolution of the liquid bridge between a fiber tip and substrate during the detaching process shows two transition points. The first transition from the radius-controlled to the contact-angle controlled process is critical to influence the strength and robustness of adhesion. We show that a concave shape is more effective than a flat one, while a convex shape has no advantage. A ring-like contact shape has advantages in a hydrophobic environment and on a rough surface.

Introduction

Insects and geckos have evolved a variety of well-defined shapes and structures for adhesion. Although often intricate and fragile, they can nonetheless deal with extreme mechanical loads with high efficiency. Some insects live attached to a substrate with dry adhesion; others use wet adhesion. These abilities are based on a variety of ingenious structural solutions. Understanding these is of great

scientific interest, since it can give insights into the workings of nature for shaping the structures in evolutionary processes. Also, we can discover the detailed chemical and physical properties of the materials which have evolved, and can learn about their use as structural elements and their biological role and function for the guidelines of man made adhesion systems.

Previous works [1–3] have studied the hierarchical structure of the animals' feet and the scaling law for dry adhesion. The adhesive system with 'dry' adhesion is based on van der Waals forces or electrostatic force between the finely structured feet and the substrate. A number of adhesion measures [4–7] on the attachment devices such as: flies, spiders, geckos, *Tettigonia viridissima*, etc, provide the evidence that van der Waals force plays dominant role in dry adhesion, and theoretical analysis [1, 8, 9] proved that biological systems indeed can use van der Waals force to achieve strong adhesion with finely structure design of the attachment systems.

In contrast, wet adhesion is based on capillary forces—through a liquid bridge between the fiber and the surface of the substrate [2]. Capillary force is a long range force in comparison with the van der Waals force. The capillary force between a hemisphere and a plane had been studied several decades ago [10]. The determination of liquid-bridge profile is the key to solve a wet adhesion problem [11]. The stability, breakage, elastic properties of liquid bridge [12] at nanometer scale are studied by both theoretical and experimental approaches. Experiments showed that humidity contributes significantly to gecko adhesion implying the importance of capillary force for adhesion at larger scale [13, 14]. A fiber-substrate model has been recently studied by Qian and Gao [15]. They find that the size of the fiber plays an important role in biological wet adhesion, and the strength of wet adhesion is

Y. Su · B. Ji (✉) · K. Hwang
Department of Engineering Mechanics, Tsinghua University,
Beijing 100084, China
e-mail: bhji@mail.tsinghua.edu.cn

Y. Huang
Department of Mechanical Science and Engineering, University
of Illinois, Urbana, IL 61801, USA
e-mail: huang9@uiuc.edu

highly enhanced by radius reduction of the fiber. A scaling law of the adhesion strength was obtained for the self-similar fiber-substrate systems.

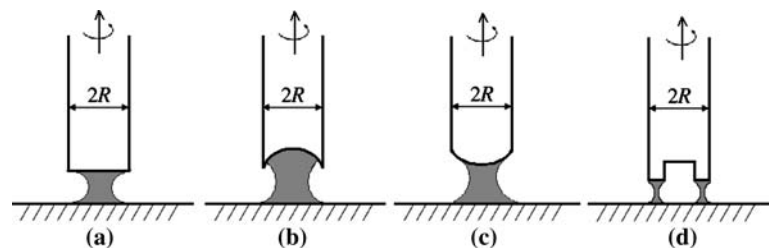
In previous studies, the tip of the fiber in the adhesion system was often assumed to be flat or hemisphere-like [16]. Experimental studies show that nature provides a variety of contact shapes, e.g., horseshoe, suction cup, and torus, etc., for good adhesion [16–21]. What is the effect of the contact shape on the adhesion force? For dry adhesion, it has been found that the contact shape exerts a strong influence on adhesion strength, e.g., the best shape is the flat tip for perfectly smooth substrate [16]. Gao and Yao [19] also discussed how to design an optimum contact shape for dry adhesion at nanoscale. In this paper, we study the effects of contact shape on the adhesion force for the wet adhesion system. This study is orientated to help improve the design of micro- and nano- manipulation system based on capillary force by the biomimicking approach. For example, recent experimental studies [21, 22] suggested that a concave tip can generate a much larger capillary force than a flat one. However, the mechanisms have not been well understood.

The organization of the paper is as follows: In Section “The model”, we introduce the models for wet adhesion with four different contact shapes of the fiber tip, mainly focusing on how to calculate the profile of the liquid bridge and the adhesion force. These four contact shapes are flat, concave, convex, and ring-like, which represent the flat punch, suction cup, hemisphere, and torus structure evolved in nature [18], respectively. In Section “Results”, these four contact shapes are studied, and the detaching force for each contact shape is calculated and compared. Finally, discussion and conclusions are made in Section “Discussion and conclusions”.

The model

The wet adhesion of the hairs of biological attachment system is modeled as a fiber contacting with the substrate mediated by a liquid bridge. To study the effect of contact shape on the adhesion strength, we introduce four different geometries of the fiber tip, i.e. flat, concave, convex, and ring-like, to model the flat punch, suction cup, hemisphere, and torus structure evolved in nature [18], respectively, shown in Fig. 1. The fiber is assumed axisymmetric. The

Fig. 1 The adhesion systems with different contact shapes. (a) flat; (b) concave; (c) convex; (d) ring-like



model for the liquid bridge is shown in Fig. 2. We make the following assumptions in order to simplify the analysis:

- No phase change such as liquid to gas during the detaching process such that the volume of liquid is conserved;
- Since the fiber and substrate are much stiffer than the liquid and therefore have essentially no deformation during the process, both the fiber and the substrate are assumed to be rigid;
- The detaching process is quasi-static such that the inertia and viscoelastic effects are negligible;
- Since the typical size (diameter) of the fiber is at the micrometer scale, the effect of gravity is negligible in comparison with the surface tension at this scale.

For this problem, the Young–Laplace equation connects the pressure difference inside and outside the meniscus to the local liquid profile by

$$\Delta P = \gamma \left(\frac{1}{R_1} + \frac{1}{R_2} \right) \quad (1)$$

where $1/R_1$ and $1/R_2$ denote the two local principal curvatures of the liquid profile, respectively, ΔP is the pressure difference which is constant within the meniscus due to the negligible gravity, and γ is interface energy between vapor and liquid. γ is connected with the contact angle θ via the Young’s equation,

$$\cos\theta = \frac{\gamma_{SV} - \gamma_{SL}}{\gamma} \quad (2)$$

where γ_{SV} and γ_{SL} are interface energy of solid–vapor and solid–liquid, respectively.

The liquid profile should be obtained first in order to calculate the adhesive force. An ordinary differential equation can be derived from Young–Laplace equation [10, 15, 23],

$$\frac{d\varphi}{ds} = \frac{\Delta P}{\gamma} - \frac{\sin\varphi}{x}, \quad \text{where } \frac{dx}{ds} = \cos\varphi, \frac{dz}{ds} = \sin\varphi \quad (3)$$

where x and z are the coordinates of the axisymmetric liquid bridge, φ is the angle between the local tangent of liquid surface and the horizontal axis, and s is the arc length of the liquid profile as shown in Fig. 2.

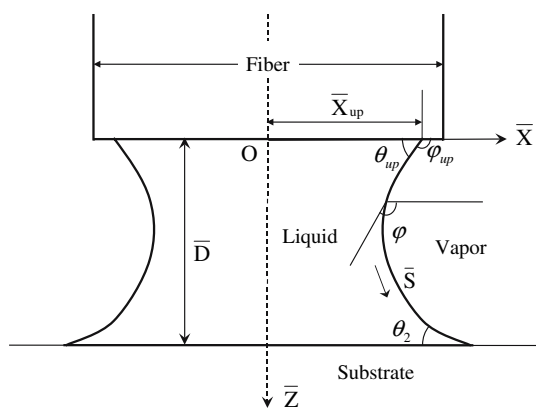


Fig. 2 The sketch map of the liquid profile and its reference frame

Introducing the nondimensional units $\bar{X} = x/R$, $\bar{Z} = z/R$, $\bar{S} = s/R$, and $\bar{H} = (\Delta P \cdot R)/\gamma$, Eq. (3) can be rewritten as,

$$\frac{d\varphi}{d\bar{S}} = \bar{H} - \frac{\sin\varphi}{\bar{X}}, \text{ where } \frac{d\bar{X}}{d\bar{S}} = \cos\varphi, \frac{d\bar{Z}}{d\bar{S}} = \sin\varphi \quad (4)$$

There are normally two states of the contact between the fiber tip and the liquid during the pulling process of the liquid bridge, i.e., radius controlled state and angle controlled state for flat contact shape [15, 24]. A critical separation \bar{D} (the distance between the fiber tip and substrate, see Fig. 2), below which the liquid periphery becomes pinned at the edge of the fiber, defines the transition point between contact angle dominated adhesion and fiber radius dominated adhesion [15, 24]. At the beginning of the detachment, the liquid profile is at the radius controlled state; as the separation becomes larger than the critical separation \bar{D} , the shrinkage of liquid contact area induces the transition from radius controlled state to angle controlled state.

In the radius controlled state, the liquid periphery is pinned at the edge of the fiber tip, and the liquid meets the surfaces of the fiber tip at the angle θ_{up} different from their real contact angle θ_1 ; \bar{X}_{up} is the radius of the contact area between the fiber and the liquid assuming the contact line is a circle (see Fig. 2). On the surface of the substrate, the liquid meets the solid always at the contact angle θ_2 as shown in Fig. 2. Therefore, the boundary conditions for the radius controlled process are,

$$\bar{X}(\bar{Z} = 0) = 1 \text{ and } \varphi(\bar{Z} = \bar{D}) = \theta_2 \quad (5a)$$

where $\varphi_{up} = \pi - \theta_{up}$, and θ_{up} can be calculated according to the separation \bar{D} .

In the angle controlled state, the liquid periphery can not touch the circumference of the fiber due to the shrinkage of the contact area when the separation between the fiber tip and substrate becomes large, then the liquid meets the fiber

surfaces at the corresponding contact angles $\theta_{up} = \theta_1$ (shown in Fig. 2). Again the liquid meets the substrate at the contact angle θ_2 . For the angle controlled process the boundary conditions are,

$$\varphi(\bar{Z} = 0) = \pi - \theta_1 \text{ and } \varphi(\bar{Z} = \bar{D}) = \theta_2 \quad (5b)$$

The liquid volume can be calculated by the following integral,

$$\bar{V} = \int_{\bar{D}} \bar{A} d\bar{Z} \quad (6)$$

And the normalized adhesion force can be calculated as follows [15],

$$\eta = -\frac{\bar{A}}{\pi} \cdot \bar{H} + \sum_i \frac{\bar{L}_i}{\pi} \cdot \sin\theta_{up}^i \quad (7)$$

where \bar{A} is the non-dimensional contact area between liquid and the fiber, \bar{L}_i is the nondimensional perimeter of contact line of the circle i . For flat, concave or convex contact tip, the contact area is a circle with one circle contact line (see Fig. 2 and 6a, b),

$$\bar{A} = \pi \cdot \bar{X}_{up}^2, \text{ and } \bar{L}_1 = 2\pi\bar{X}_{up}, \quad i = 1 \quad (8)$$

however, for ring-like contact shape (Fig. 6c), the contact area is annular with two circle contact lines,

$$\bar{A} = \pi(\bar{X}_{up}^{out^2} - \bar{X}_{up}^{in^2}), \quad \bar{L}_1 = 2\pi\bar{X}_{up}^{out} \text{ and } \bar{L}_2 = 2\pi\bar{X}_{up}^{in}, \quad i = 1, 2 \quad (9)$$

Table 1 in the Appendix gives the analytical solutions for the axisymmetric profile of the liquid bridge in curvilinear coordinates for the calculation of the liquid volume and the separation.

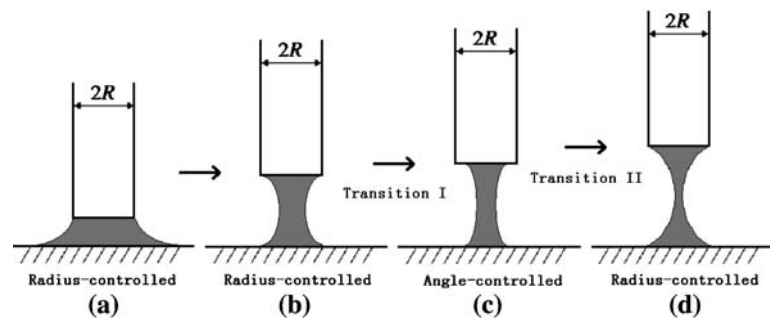
Results

We first study the detaching process of a fiber with flat tip from the substrate, focusing on the details of the separating process, such as the transition points between the two states, and the relation between transition points and the point for the maximum detaching force. We then study the detaching process of the fiber with other three contact shapes, i.e., concave, convex, and ring-like.

Flat tip

The prior study [15, 23] on the mechanics of wet adhesion of a cylindrical fiber with flat tip to an infinite substrate

Fig. 3 A typical separating process of the fiber-liquid-substrate system with a flat tip which shows the evolution of the profile of the liquid as the contact state between fiber and liquid changes from radius controlled to angle controlled, and then comes back to radius controlled state before the liquid collapses



focused on the scaling effects in adhesion force. The size reduction of the fiber and liquid bridge (i.e., the radius of fiber and volume of liquid) as well as small contact angle increase the adhesion strength. The present work focuses on the influence of contact shape on the adhesion force. We first examine the evolution of liquid bridge profile, and its contact area with both the fiber and the substrate during the detaching process in order to identify the mechanisms of enhancing the adhesion strength via the contact shape.

A typical separating process of liquid bridge between a fiber with flat tip and substrate is shown in Fig. 3. There are two transition points during the detaching process. The first is the radius controlled to angle controlled state transition; the second one is angle-to-radius controlled transition, which has not been reported before. At the beginning of the detachment, the normalized detaching force η (capillary force) is negative because the part of total detaching force due to the pressure difference is negative and its absolute value is larger than the part due to the surface tension of the liquid at small separation (see Eq. 7). With the increase of the separation, the detaching force continuously increases and becomes positive, then reaches its maximum value at a critical point; afterwards, the capillary force decreases as the separation increases, as shown in Fig. 4a. The position of the two transition points is of great interest for small contact angle θ_1 . For example, for $\theta_1 = 0$, the radius-to-angle controlled transition (transition I) occurs after the critical point for the maximum capillary force; and the transition II, i.e., the angle-to-radius controlled transition occurs near the critical point of breakage of the liquid bridge. These are further illustrated in Fig. 4b, c, which show the evolution of the contact angle and contact radius between the fiber and liquid, respectively. In particular, Fig. 4c clearly shows the shrinkage and then spreading process of the contact area between the two transition points. We define the maximum value of the detaching force as the ideal maximum detaching force when the transition I happens after the critical point for the maximum detaching force. When the transition I happens earlier than the critical point (at larger θ_1), the maximum detaching force is smaller than the ideal maximum detaching force as shown in Fig. 5.

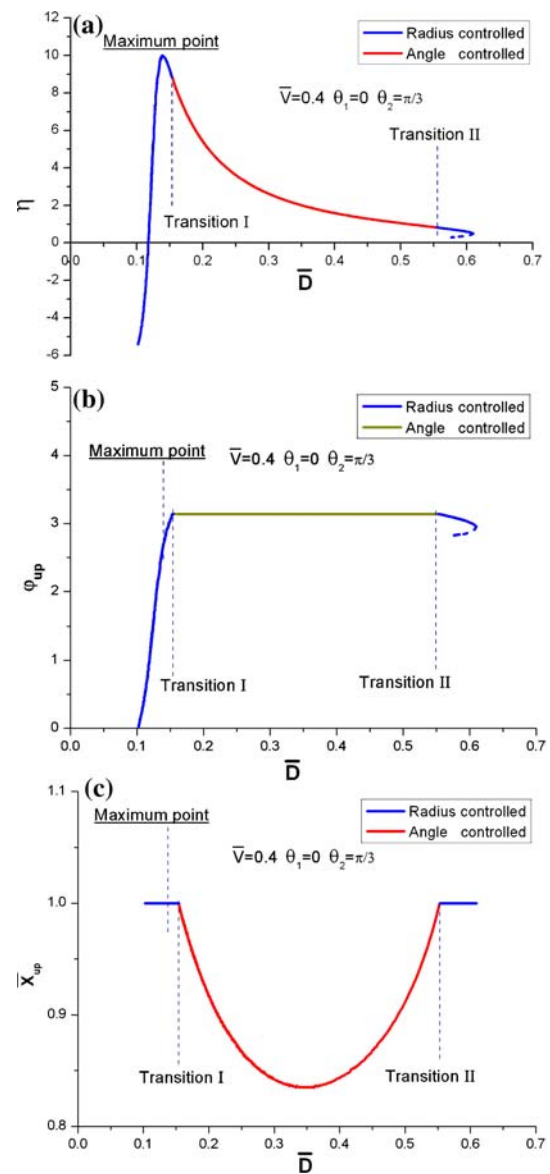


Fig. 4 (a) The force-separation curve of the liquid bridge in a quasi-static pulling process, showing two contact states and their transition points; (b) the evolution of the angle between the fiber surface and liquid ϕ_{up} during the pulling process; (c) the evolution of the normalized radius of contact area \bar{X}_{up}

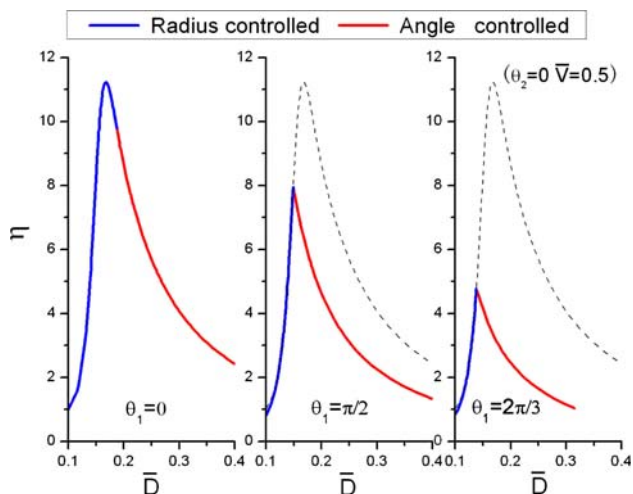


Fig. 5 The force-separation curves for the flat shape with different contact angle θ_1 , which shows that the larger the θ_1 , the earlier the happening of the transition I, and the smaller the adhesion force is

The positions of the transition points on Fig. 4a depend on the liquid volume and the two contact angles θ_1 and θ_2 . Our numerical results show that the increase of contact angle θ_1 brings transition I forward (see Fig. 5). Once the transition-I point reaches the critical point for the ideal maximum detaching force, the detaching force starts to decrease, and the maximum detaching force becomes smaller than the ideal maximum adhesion force as shown in Fig. 5. Therefore, transition I is crucial for the detaching force, and the contact angle θ_1 influences the transition-I position. For θ_1 smaller than a critical value, the transition I always happens after the critical point for the ideal maximum detaching force such that the maximum detaching force is equal to the ideal maximum detaching force, as shown by the red dashed line and the curve of the flat tip in Fig. 8. We define this critical value of the contact angle θ_1 as θ_1^* below which the detaching force can achieve its ideal maximum value. This mechanism is important to the understanding of detaching process of fiber with other contact shapes, such as concave and convex tip, as to be shown later.

Concave and convex tip

For the study of detaching process of the fiber with the concave shape, we first introduce the concept of the effective contact angle and effective liquid volume for the convenience of comparing with the flat shape. The effective contact angle θ_{eq} is defined as the angle between the tangent line of the liquid profile (two dimensional) and the horizontal line at the triple point (of solid, liquid and vapor), as shown in Fig. 6a, and $\theta_{eq} < \theta_1$ for the concave shape. The effective liquid volume \bar{V}_{eq} is defined as the volume of liquid under the horizontal plane passing the outer edge of the concave surface (see Fig. 6a). However, the total volume of the liquid bridge under the concave surface is $\bar{V} = \bar{V}_{eq} + \Delta\bar{V}$, where $\Delta\bar{V}$ is the volume between the horizontal plane and the concave surface, as shown in Fig. 6a.

The numerical results show that the concave tip can induce larger detaching force than the flat tip under the condition of the same effective liquid volume at large contact angle θ_1 ($\theta_1 > \theta_1^*$). Here the effective liquid volume for flat shape is the same as its total volume. The detaching forces for the concave, flat and convex tips are shown in Fig. 7 by the curves A, B and C, respectively, for the liquid volume $\bar{V} = \bar{V}_{eq} = 1.0$. The maximum detaching force for the concave shape is larger than that for the flat tip, while the convex tip gives the smallest. What is the mechanism for the concave shape to achieve large detaching force? It is observed that all three curves overlap before the detaching force for the convex shape reaches its maximum value, after which the detaching force for the convex tip decreases, followed by the flat tip, but the force for the concave shape continues to increase and reaches its maximum value higher than that of the flat shape at a larger separation \bar{D} . The underlying mechanism is that the concave shape delays the radius-to-angle controlled transition, which effectively increases the detaching force.

In order to further understand this mechanism, we study the relationship between the contact angle θ_1 and the

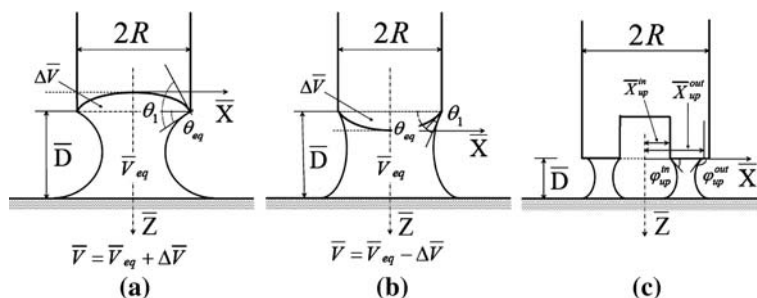


Fig. 6 Schematic illustration of the fiber-liquid-substrate system with three different shapes. (a) the concave shape with an effective contact angle $\theta_{eq} < \theta_1$ and an effective liquid volume $\bar{V}_{eq} = \bar{V} - \Delta\bar{V}$; (b) the

convex shape with an equivalent contact angle $\theta_{eq} > \theta_1$ and an effective liquid volume $\bar{V}_{eq} = \bar{V} + \Delta\bar{V}$; (c) the ring-like contact shape with two contact lines

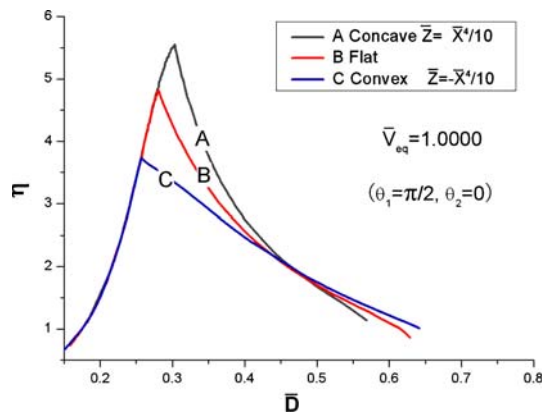


Fig. 7 The comparison of the detaching force among different contact shapes, concave, convex and flat shape. The figure shows that the concave shape can induce larger detaching force than that with flat and the convex shape under the condition of the same effective liquid volume

maximum detaching force for the concave shape. The comparison of the maximum force between the concave shape with $\bar{Z} = \bar{X}^{10}/4$ and $\bar{Z} = \bar{X}^2/4$, and the flat shape at same effective liquid volume, is shown in Fig. 8. For the flat shape, the maximum detaching force remains a constant and is equal to the ideal maximum detaching force when $\theta_1 < \theta_1^* = 20^\circ$, but starts to decrease when $\theta_1 > 20^\circ$. The concave shape achieves the same ideal maximum detaching force, but its critical value θ_1^* is much larger than that of the flat shape, such as $\theta_1^* = 45^\circ$ for the concave shape $\bar{Z} = \bar{X}^2/4$. This implies that the concave shape is less sensitive to the changing of contact angle θ_1 , and reflects the “robustness” of the adhesion system [3, 19, 25] about the surface chemistry of material. For further increased curvature of the concave-shaped fiber tip, $\bar{Z} = \bar{X}^{10}/4$, the maximum force

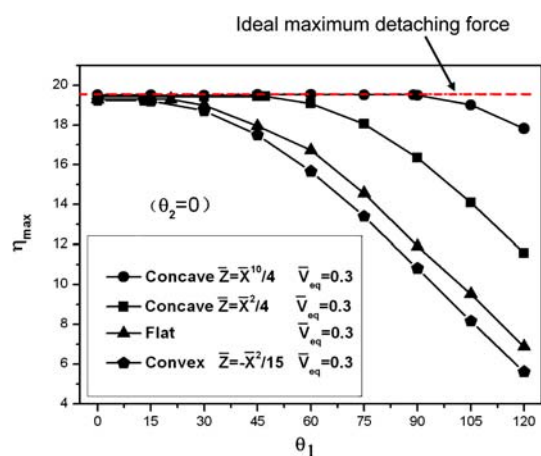


Fig. 8 The relationship between the maximum detaching force and the contact angle θ_1 for different contact shapes: concave $\bar{Z} = \bar{X}^{10}/4$, concave $\bar{Z} = \bar{X}^2/4$, convex $\bar{Z} = -\bar{X}^2/15$ and the flat shape. It shows that the concave shape make the maximum detaching force be insensitive to the change of contact shape θ_1

does not decrease until the contact angle is increased to as large as $\theta_1 = 90^\circ$, and only has a minor decrease at the contact angle $\theta_1 = 120^\circ$, exhibiting stronger robustness. This shows that the large curvature at the contact edge of the concave shape can effectively enlarge the critical value of θ_1^* (retarding effect) for the radius-to-angle controlled transition so that the transition can not happen and therefore the ideal maximum detaching force can always be achieved in a very large region of θ_1 . It can be seen from Fig. 8 that the larger the curvature of the concave shape, the more effective the retarding effect it has.

In the same manner of studying the detaching process of the fiber with the concave tip, we consider the effect of the convex contact shape on the wet adhesion. Our calculations show that the detaching force for the convex tip is more sensitive to the contact angle θ_1 in comparison with the concave shape and flat shape, see Fig. 8. The mechanism is that the effective contact angle between the fiber and liquid for the convex shape is larger than their real contact angle, $\theta_{eq} > \theta_1$ due to the negative curvature of the contact surface (see Fig. 6b, while $\theta_{eq} < \theta_1$ for concave shape) and thus promotes the transition I to occur earlier, which severely weakens the adhesion force. For instance, the detaching force of a convex tip described by $\bar{Z} = -\bar{X}^2/15$ is calculated and compared with that of the flat and concave shape in Fig. 8. From Fig. 8, we can see that the detaching force for the convex tip can only achieve the ideal maximum detaching force at very small region of the contact angle θ_1 and declines much faster with the increase of the contact angle in comparison with the flat and concave tip. Therefore, we conclude that the convex shape is less efficient for the wet adhesion.

Ring-like tip

Our previous calculations have shown that, at small contact angle, the adhesion force of the fiber-substrate system with flat, concave and convex contact shape mainly relies on the pressure difference ΔP ; however, for large contact angles θ_1 and θ_2 , i.e., the surface of fiber tip and the substrate are hydrophobic, the pressure difference can be positive, which largely decreases the detaching force. In order to enhance the adhesion force in a hydrophobic environment, the contact area should be reduced, but the contact line length should be enlarged to strengthen the detaching force via surface tension. The ring-like contact shape should be a good candidate.

The detaching force of the ring-like contact shape in comparison with the flat shape at various liquid volume is shown in Fig. 9. The ring-like contact shape is clearly a better choice than the flat shape at a hydrophobic environment (i.e., at large contact angle θ_2); we can see that the ring-like shape induces a larger detaching force at a larger separation for small liquid volume because its force-separation

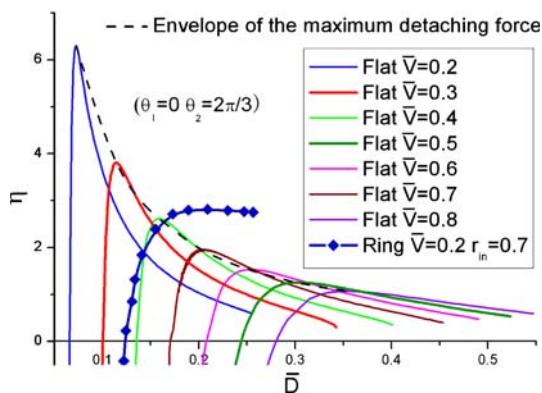


Fig. 9 The force-separation curve of the ring-like contact shape in a hydrophobic environment (large θ_2) in comparison with the envelope of the force-separation curves of the flat shape with various liquid volume, where the contact angle $\theta_1 = 0$. It shows that the ring-like contact shape can achieve comparably larger detaching force at larger separation in a hydrophobic environment

curve is above the envelop of those of the flat tip for different liquid volume (see Fig. 9). Although the maximum detaching force of the flat shape at volume $\bar{V} = 0.2$ is larger than that of the ring-like contact shape, this maximum is achieved at very small separation, $\bar{D} < 0.1$; for a rough surface with $\bar{D} > 0.1$, this maximum detaching force may not be achievable. Consequently, the ring-like contact shape may enhance the adhesive force in the hydrophobic environment.

Discussion and conclusions

This paper is aimed to study the effect of different contact shapes on the detaching force in order to provide the guidelines for the design of the micro- and nano- attachment system through biomimicking approach. For a fiber with flat tip, there are two transition points of the contact state between the fiber tip and the liquid bridge, i.e., the

radius-to-angle controlled transition (transition I) and the angle-to-radius controlled transition (transition II), where the second transition is identified for the first time in this paper. The transition I is crucial for the maximum detaching force. The detaching force always achieves its ideal, maximal value if the transition I occurs after a critical point. There also exists a critical value for the contact angle between the fiber and liquid for the transition I at which the detaching force reaches its Ideal maximal value. In comparison with the flat tip, the concave contact shape is more effective to delay the transition I and therefore to achieve the maximum detaching force. The concave tip also makes the detaching force be insensitive to the changing of contact angle, and therefore is robust to the chemical change of the environment. This finding is consistent with the experimental observations [21, 22] of the attachment system of flies to explain why nature designs the concave tip for wet adhesion. Furthermore, we show that a convex contact shape has no such advantage, and a ring-like contact shape has advantages for a rough surface in a hydrophobic environment. The present work represents the first systematically study of the effect of contact shape on wet adhesion of biological attachment systems, which paves the way for the optimum design of the contact shape of wet adhesion systems, and may be used in the bio-inspired design of new mechanical microsystems (such as MEMS/NEMS). Knowledge gained from these studies will not only extend our insights concerning biological adhesion, but these results may also prove indispensable in practical applications.

Acknowledgments This work is supported by the National Natural Science Foundation of China through Grant No. 10442002, 10502031, 10628205, 10121202, Tsinghua Basic Research Foundation, and National Basic Research Program of China through Grant No. 2004CB619304, and SRF for ROCS, SEM.

Appendix

Table 1 Analytical solution of the axisymmetric liquid profile

Meridional curvature	Average curvature	Profile radius	Profile radius	Remark
a $\frac{d\phi}{d\bar{s}} > 0$	$\bar{H} \neq 0$	$\bar{X} > 0$	$\bar{X}(\phi) = \frac{\sin\phi + \sqrt{\sin^2\phi + \bar{H}\bar{X}_{up}(\bar{H}\bar{X}_{up} - 2\sin^2\phi_{up})}}{\bar{H}}$	

Table 1 continued

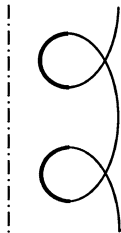





Meridional curvature	Average curvature	Profile radius	Profile radius	Remark
b $\frac{d\varphi}{dS} < 0$	$\bar{H} \neq 0$	$\bar{X} > 0$	$\bar{X}(\varphi) = \frac{\sin\varphi - \sqrt{\sin^2\varphi + \bar{H}\bar{X}_{up}(\bar{H}\bar{X}_{up} - 2\sin\varphi_{up})}}{\bar{H}}$	
c $\frac{d\varphi}{dS} < 0$ or $\frac{d\varphi}{dS} = 0$ or $\frac{d\varphi}{dS} < 0$	$\bar{H} \neq 0$	$\bar{X} > 0$	$\bar{X}(\varphi) = \begin{cases} \frac{\sin\varphi + \sqrt{\sin^2\varphi + \bar{H}\bar{X}_{up}(\bar{H}\bar{X}_{up} - 2\sin\varphi_{up})}}{\bar{H}} \frac{d\varphi}{dS} > 0 \\ \frac{\sin\varphi - \sqrt{\sin^2\varphi + \bar{H}\bar{X}_{up}(\bar{H}\bar{X}_{up} - 2\sin\varphi_{up})}}{\bar{H}} \frac{d\varphi}{dS} < 0 \end{cases}$ Inflection $\begin{cases} \bar{X}_c^2 = -\frac{\bar{X}_{up}}{\bar{H}}(\bar{H}\bar{X}_{up} - 2\sin\varphi_{up}) > 0 \\ \sin^2\varphi_c = -\bar{H}\bar{X}_{up}(\bar{H}\bar{X}_{up} - 2\sin\varphi_{up}) = \bar{M}(0 < \bar{M} \leq 1) \end{cases}$	
d $\frac{d\varphi}{dS} = 0$ (global)	$\bar{H} \neq 0$	$\bar{X} > 0$	$\bar{X} = \frac{1}{\bar{H}} \quad \varphi = \frac{\pi}{2}$	
e $\frac{d\varphi}{dS} = 0$ (global)	$\bar{H} = 0$	$\bar{X} > 0$	$\sin\varphi = 0$ ($\varphi = 0$ or $\varphi = \pi$)	
f $\frac{d\varphi}{dS} \neq 0$ or $\frac{d\varphi}{dS} = 0$ (local)	$\bar{H} = 0$	$\bar{X} > 0$	$\bar{X}(\varphi) = \frac{\bar{X}_{up}\sin\varphi_{up}}{\sin\varphi}$	

Table 1 continued

Meridional curvature	Average curvature	Profile radius	Profile radius	Remark
$g \frac{d\phi}{ds} \neq 0$	$\bar{H} \neq 0$	$\bar{X} = 0$ (local)	$\bar{X}(\phi) = \frac{2\sin\phi}{H}$ $\bar{Z}(\phi) = -\frac{2\cos\phi}{H}$	

Note: Meridional curvature refers to $\frac{d\phi}{ds} = \bar{H} - \frac{\sin\phi}{\bar{X}}$, ‘Local’ means position of a point or several points, and ‘global’ means the whole line of the liquid profile

References

- Gao H, Wang X, Yao H, Gorb S, Arzt E (2005) *Mech Mater* 37:275
- Federle W, Riehle M, Curtis ASG, Full RJ (2002) *Integr Comp Biol* 42:1100
- Gao H, Ji B, Buehler MJ, Yao H (2004) *Mol Cel Biol* 1:37
- Jiao YK, Gorb S, Scherge M (2000) *J Exp Biol* 203:1887
- Gorb S, Gorb E, Kastner V (2001) *J Exp Biol* 204:1421
- Autumn K, Peattie AM (2002) *Integr Comp Biol* 42:1081
- Kesel AB, Martin A, Seidl T (2004) *Smart Mater Struct* 13: 512
- Autumn K, Sitti M, Liang YCA, Peattie AM, Hansen WR, Sponberg S, Kenny TW, Fearing R, Israelachvili JN, Full RJ (2002) *Proc Natl Acad Sci U S A* 99:12252
- Arzt E, Gorb S, Spolenak R (2003) *Proc Natl Acad Sci USA* 100:10603
- Orr FM, Scriven LE (1975) *J Fluid Mech* 67:723
- Rabinovich YI, Adler JJ, Esayanur MS, Ata A, Singh RK, Moudgil BM (2002) *Adv Colloid Interface Sci* 96:213
- Choe H, Hong MH, Seo Y, Lee K, Kim G, Cho Y, Ihm J, Jhe W (2005) *Phys Rev Lett* 95
- Huber G, Mantz H, Spolenak R, Mecke K, Jacobs K, Gorb SN, Arzt E (2005) *Proc Natl Acad Sci USA* 102:16293
- Sun WX, Neuzil P, Kustandi TS, Oh S, Samper VD (2005) *Biophys J* 89:L14
- Qian J, Gao HJ (2006) *Acta Biomater* 2:51
- Spolenak R, Gorb S, Gao H, Arzt E (2005) *Proc R Soc London Ser A-Math Phys Eng Sci* 461:305
- Federle W, Brainerd EL, McMahon TA, Holldobler B (2001) *Proc Natl Acad Sci USA* 98:6215
- Gorb S, Jiao YK, Scherge M (2000) *J Comp Physiol A-Sens Neural Behav Physiol* 186:821
- Gao H, Yao H (2004) *Proc Natl Acad Sci USA* 101:7851
- Scherge M, Gorb SN (2000) *J Micromech Microeng* 10:359
- Langer MG, Ruppertsberg JP, Gorb S (2004) *Proc R Soc Lond Ser B-Biol Sci* 271:2209
- Saito S, Motokado T, Obata KJ, Takahashi K (2005) *Appl. Phys Lett* 87
- Obata KJ, Motokado T, Saito S, Takahashi K (2004) *J Fluid Mech* 498:113
- Fortes MA (1982) *Powder Metall Int* 14:96
- Gao H, Ji B, Jager IL, Arzt E, Fratzl P (2003) *Proc Natl Acad Sci USA* 100:5597